Preparation and Characterization of Polyfluorene-Based Supramolecular π-Conjugated Polymer Gels

ARTICLE *in* THE JOURNAL OF PHYSICAL CHEMISTRY C · MARCH 2011

Impact Factor: 4.77 · DOI: 10.1021/jp109598y

10 AUTHORS, INCLUDING:

Yi-bao Li
Gannan Normal University
40 PUBLICATIONS **586** CITATIONS
SEE PROFILE

Dong Qiu
Chinese Academy of Sciences
74 PUBLICATIONS **774** CITATIONS
SEE PROFILE

Ling-Hai Xie
Nanjing University of Posts and Telecommu…
149 PUBLICATIONS **1,979** CITATIONS
SEE PROFILE

Wei Huang
University of Hawai'i at Mānoa
1,349 PUBLICATIONS **30,748** CITATIONS
SEE PROFILE

THE JOURNAL OF PHYSICAL CHEMISTRY C

ARTICLE

pubs.acs.org/JPCC

Preparation and Characterization of Polyfluorene-Based Supramolecular π-Conjugated Polymer Gels

Zong-Qiong Lin,[†] Nai-En Shi,[‡] Yi-Bao Li,[§] Dong Qiu,[∥] Long Zhang,[‡] Jin-Yi Lin,[‡] Jian-Feng Zhao,[†] Chen Wang,[§] Ling-Hai Xie,[*,‡] and Wei Huang[*,†]

[†]Key Laboratory for Organic Electronics & Information Displays (KLOEID) and [‡]Institute of Advanced Materials (IAM), Nanjing University of Posts and Telecommunications, 9 Wenyuan Road, Nanjing 210046, China

[§]National Center for Nanoscience and Technology, Beijing 100190, China

[∥]Beijing National Laboratory for Molecular Sciences, State Key Laboratory of Polymer Physics and Chemistry, Institute of Chemistry, Chinese Academy of Sciences, Beijing 100190, China

Supporting Information

ABSTRACT: Supramolecular π-conjugated polymer-based gels (SCPGs) are one important kind of semiconducting soft materials. Herein we demonstrate a poly(9,9-dioctylfluorene) (PFO) based on SCPG in 1,2-dichloroethane (DCE). The PFO/DCE gel exhibits a characteristic photoluminescence profile distinguished from other polymorphisms. The emission peak at ca. 550 nm evidences the aggregate or excimer mechanism of the low-energy emission band in polyfluorenes. Thermoreversible sol−gel transition of PFO/DCE gel has been investigated by temperature-resolved fluorescence spectroscopy and differential scanning calorimetry (DSC). The formation mechanism of PFO/DCE gel has been proposed according to the scanning tunneling microscopy (STM) and small-angle X-ray scattering (SAXS) analysis. The obtained xerogel via freeze-drying exhibited regularly interpenetrated pores with the size of about 2−5 μm. Gelation of π-conjugated polymers paves a promising way to prepare porous soft semiconductors with potential applications of sensors and actuators.

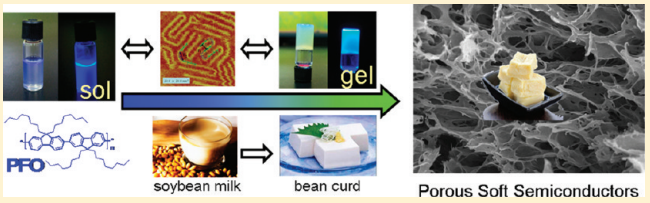

INTRODUCTION

During the past decades, π-conjugated polymers have been studied intensively owing to their potential applications in organic optoelectronic devices, such as polymeric light-emitting diodes, bulk heterojunction solar cells, organic field-effect transistors (OFETs), organic memories, biosensors, and actuators.[1,2] The performance of organic devices is determined not only by the inherent electronic structures of individual polymer chain[3,4] but also by multiscale morphologies that were constructed by the drive of supramolecular interactions or van der Waals' forces. Many efforts have been made to design the controllable well-defined nanostructures or hierarchically ordered assemblies in the field of supramolecular semiconductors and electronics for the high-performance or new functional devices.[5,6] One typical example is that ordered self-organization of polythiophenes dramatically influences the performance of bulk heterojunction photovoltaic cells as well as the mobility of OFETs.[7,8] Light-emitting polyfluorenes (PFs) is another impressive example of polymorphisms, including amorphous phase, semicrystalline (α-) phase and α′-phase, β-phase, and nematic liquid crystalline (N-) phase. These abundant phases provide a unique opportunity to study the relationship between phase morphology and device performances.[9−13] For example, PFO thin film containing the β-phase exhibits the excellent spectral stability in PLEDs and the pumped lasers with low threshold.[14−16] In this context, it is of the utmost importance to explore further the unique morphology and phase of π-conjugated polymers, which are based on its unique self-assembly mode and supramolecular interactions.

Supramolecular gel is a fascinating state that appears solid-like and yet is composed predominantly of a liquid and a small amount of gelators stabilized by supramolecular interactions with 3D networks.[17−20] Until now, low-molecular-mass organogels (LMOGs) have been applied in a wide range of fields, such as biomimetics, separations, drug delivery, soft templates, and tissue engineering.[21−24] Steroid or lipid units have served as gelators to generate cross-linking points in the 3D networks.[25] In addition, some electronically inactive comb-shaped polymers (isotactic and syndiotactic polystyrene (PS),[26] poly(methyl methacrylate),[27] and polyesters[28]) have also been found to form gel networks easily owing to their unique helical conformations. However, little attention has been paid to π-conjugated polymers.[29−32] Supramolecular π-conjugated polymer gels (SCPGs) can be served as one kind of semiconducting soft materials with distinguished porous structures that may find applications in nanosensors,[33] mimic-artificial muscle,[34] super capacitor,[35] and lithium battery material.[36] Poly(3-alkylthiophene)-based gels were prepared by quenching xylene solution at 150 °C, and its conductivity was improved.[37,38]

Received: October 7, 2010
Revised: December 26, 2010
Published: March 03, 2011

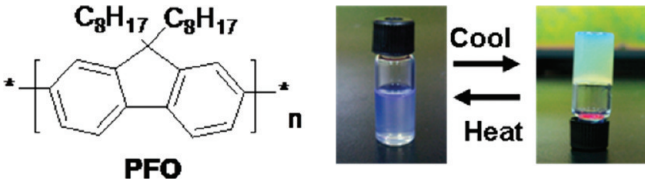

Figure 1. Chemical structure of PFO and photograph of PFO/DCE gel.

Poly[2-methoxy-5-(2-ethylhexyloxy)-1,4-phenylenevinylene] (MEH-PPV) formed a soft gel after storing for several weeks in toluene or addition of alkanes at low or room temperature.,[39] Oligo(*p*-phenylenevinylene)s gel with hierarchical self-assembly mode in nonpolar solvents has also been reported by Ajayaghosh et al.[40] PFO-based gels were first reported by Bradley et al. and further investigated by Chen et al. using dynamic light scattering and photoluminescence (PL).[41−43] It is still a challenge for π-conjugated polymers to understand the gelating mechanism and expand their applications. In this research, we have successfully prepared PFO-based supramolecular π-conjugated polymer-based gel (**PFO-SCPG**) in 1,2-dichloroethane (DCE). Its sol−gel transition process has been investigated by UV-vis, PL spectra, differential scanning calorimeter (DSC), scanning tunneling microscopy (STM), and small-angle X-ray scattering (SAXS). PFO/DCE gel exhibits the unique PL behaviors that are greatly distinguished from any other polymorphism of PFO. The excellent macroporous architectures of PFO Xerogel may serve as a promising candidate for the sensors and actuators.

RESULTS AND DISCUSSION

Preparation of PFO-SCPG. The chemical structure of PFO and the photograph of PFO/DCE gel are shown in Figure 1. PFO/DCE gel was prepared by a typical heating−cooling process, in which PFO with a typical concentration of 5 mg·mL^{-1} was heated to ca. 80 °C for 3 h, left it stand, and cooled to room temperature for 24 h. Under the same condition, we also made an attempt to utilize other solvents with different Hildebrand solubility parameter (δ)[43,44] and boiling points, including dichloromethane (DCM), chloroform, chlorobenzene (CB), *n*-hexane, and toluene. It was found that DCE was the only solvent to gelate PFO. It should be noted that PFO/DCE gel can be formed more easily as compared with PFO/toluene gel obtained at low temperature of −20 °C.[42] In addition, methylcyclohexane (MCH) or cyclohexane with the solubility parameters of 7.8 and 8.2 (cal/cm^3)$^{1/2}$, respectively, also induced the gelation of PFO at room temperature.[41,45] It is believed that a suitable solubility of the solvent is the key requirement to generate physical cross-linked networks of polymer. PFO exhibits Hildebrand solubility parameter δ of 9.1−9.3 (cal/cm^3)$^{1/2}$.[41] DCE with the solubility parameter value of 9.8 (cal/cm^3)$^{1/2}$ shows a moderate solubility relative to PFO. It is reasonable that gel was obtained in neither chloroform with pretty good solubility with PFO nor extraordinary poor solvents, such as *n*-hexane.[46] In addition, besides the solubility parameter, the boiling point of solvent also plays a vital role in the gel formation. For example, precipitation rather than gelation was observed using DCM (as a moderate solvent), whose solubility approximates to that of DCE.

Optical Properties of PFO-SCPG. To investigate further the properties and formation processes of the PFO/DCE gel, its UV-vis absorption and PL spectra have been characterized. Electronic absorption spectra of dilute DCE solution (~2 μg/mL), the PFO/DCE gel, the dip-processed film, and the film spin-coating from DCE are shown in Figure 2. It should be noted that the dip-processed film is obtained by dipping the pristine film that spin-coated from chloroform solution into DCE for 20 s. β-Phase of PFO is an isomer planar conformation with an extended conjugation length,[41,47−49] which can be probed by the characteristic peak of 437 nm in UV−vis absorption spectra.[50] In PFO/DCE dilute solution (~2 μg/mL), there is a weak absorption peak at 437 nm, that is a small fraction of β-phase of PFO in the diluted solution (Figure 2). The peak of β-phase at 437 nm is relatively strong in the thin film, which spin-coated from DCE hot solution. Dipping processes of film spin-coated from chloroform without β-phase into DCE also induced the high content of β-phase. Furthermore, PFO/DCE gel shows the higher content of β-phase than the above-mentioned states (can be >50%, see the Supporting Information). These results indicated that DCE solution benefited from the formation of β-phase, which is probably the key intermediate in the formation of gel. To make a quantitative contrast of the influence of solvents, β-phase contents of dip-processed film and drop-cast films using various solvents, including DCE, toluene, *n*-hexane, CB, DCM, and chloroform, have been summarized. (See the Supporting Information). With respect to the other solvent, the film obtained from DCE solution exhibited the highest β-phase contents, which suggested that the moderately poor DCE is the most effective solvent to induce the formation of β-phase in solution, film, or both. These results support the point that the high content of β-phase is favorable for the gel formation according to the literature reported by Grell et al.[41]

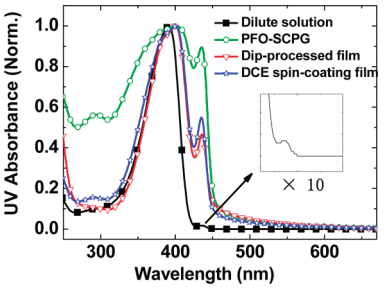

Figure 2. UV-vis absorption spectra of PFO in DCE dilute solution, gel, dip-processed film (preparing by dipping the pristine film which spin-coated from chloroform solution into DCE for 20 s), and the film spin-coated from DCE solution.

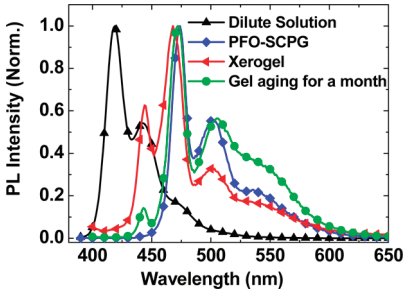

Figure 3. Photoluminescence spectra of PFO in dilute solution of DCE, gel, and aging gel as well as xerogel.

PL spectra of PFO in DCE dilute solution, gel, and gel aging for a month at ambient temperature as well as xerogel are shown in Figure 3. For the PFO/DCE dilute solution, there are three

dx.doi.org/10.1021/jp109598y |J. Phys. Chem. C 2011, 115, 4418–4424

emission bands at 419, 443, and 472 nm, assigned to the 0−0, 0−1 and 0−2 intrachain singlet transition according to the literature, which indicates that PFO chains are well-dissolved in the isotropic phase.[47] The characteristic emission bands of PFO/DCE gel are located at 473 and 500 nm with a concomitant broad emission band at 550 nm, which distinguished from isotropic phase, β-phase, as well as other polymorphisms. PFO in the β-phase has the featured peaks at 446, 473, and 500 nm according to the reports by Khan et al., corresponding 0−0, 0−1, and 0−2 vibrational transitions of β-phase.[47] In contrast with the 0−0 transition peak at 446 nm of β-phase, a red shift of 27 to 473 nm occurs in the 0−0 transition of PFO/DCE gel. It is interesting that this peak at 473 is close to the second peak of β-phase, which indicates that a new aggregate architecture is formed, resulting in the complete energy transfer from the 0−0 vibration of β-phase. This architecture probably involved with the physically cross-linked 3D networks with the shorter $\pi-\pi$ stacking distance of fluorene segments.[41,52] It should be noted that the PFO/DCE gel spectrum is slightly different from that of PFO/toluene reported by Chen,[42] in which 0−0 emission band of β-phase still exists in the previous reports, whereas a much weaker at 550 nm was observed. After the PFO/DCE gel was aged for a month, the PFO/DCE gel shows that the peak at 446 nm from β-phase reappears, and the peak intensity of 550 nm increased. Similarly, PFO xerogel also exhibits the four emission peaks at 446, 473, 500, and 550 nm. The difference is only that emission of the β-phase at 446 nm is stronger than that of aging gel, and the peak at 550 nm is weaker than that of fresh gel. These results are further evidence of the energy transfer from β-phase to gel state. In the xerogel, it can be interpreted as a fraction of π-stacked fluorene segments disassembled during the freeze-drying, and the effective Förster energy transfer from isotropic polymers to the network is prevented by the increased distance.

PFO/DCE gel affords a unique model to illustrate the controversial low-energy green emission bands centered at 520−550 nm in PFs. The band at 550 nm can be explained by the fact that a relatively tight gel networks in DCE was formed and effectively increased the $\pi-\pi$ stacking interaction of fluorene segments by overcoming the steric hindrance of the pendant dioctyl groups at the nine-position of fluorene. The origins of the low-energy green band emission are still controversial between two main mechanisms, that is, the aggregate (or excimer) and keto-defects.[52−56] Until now, there are only a few supporting works in which the green band originates from intermolecular aggregates or excimers. For example, Su et al. reported self-condensed nanoparticles of oligofluorenes with amphiphilic side chains to give a sharp green emission in THF/H_2O.[57] Here the green emission band at 550 nm of PFO/DCE gel probably supported the excimer mechanism because the mechanism of "keto-defects" can be easily eliminated in PFO/DCE gel. First of all, the PL profiles are unique and reversible by thermal circulations, which are distinguished from the copolymers comprising fluorenone reported by Jaramillo-Isaza,[58] Panozzo,[59] and Liu et al.[60] No distinct green emission was observed in the spin-coating film of PFO/DCE sol from gel with the peak of 550 nm. Furthermore, featuring peak of ketone at 1720 cm^{-1} in the FT-IR spectra[60,61] was not observed (Supporting Information), either. Therefore, the PFO/DCE gel affords another system to support the probability of the aggregate mechanism of low-energy green emission band.[62,63]

Thermoreversible Sol−Gel Transition Process. The thermoreversible sol−gel transition process of the PFO/DCE gels is easily visible to the naked eye, which was also examined by DSC and temperature-resolved PL experiment. DSC curves of PFO/DCE gel are shown in Figure 4. In the first heating cycle from 30 to 80 °C, an endothermic process took place in the range of 65 to 68 °C with a sharp peak at 66 °C. The endothermic peak in DSC suggests that the transition occurs from physical cross-linked network to isotropic phase of PFO. However, neither exothermic nor endothermic process was observed during the cooling process, which indicates that PFO/DCE sol cannot be rapidly reconstructed into gel in such a short time. A similar curve of DSC can be observed after 24 h of aging, indicating the excellent reversibility of gel−sol transition. (See the Supporting Information.)

The detailed sol−gel transition process of thermoreversible PFO/DCE gel can be further characterized by the temperature-resolved PL, together with the camera photograph of the sol−gel transition under UV lamp with the irradiation wavelength of 365 nm, as shown in Figure 5. Figure 5a shows four different types of fluorescence profiles reflecting the transition process of the PFO/DCE gelation system (5 mg·mL^{-1}). First, the PL spectrum at the temperature of 80 °C shows an emission peak at

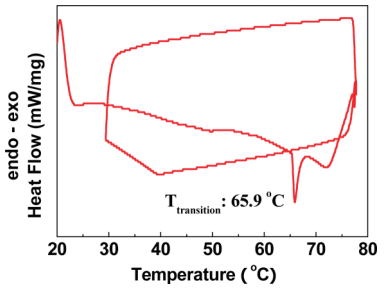

Figure 4. DSC data of PFO/DCE gel from 30 to 80 °C at the scanning speed of 5 °C/min.

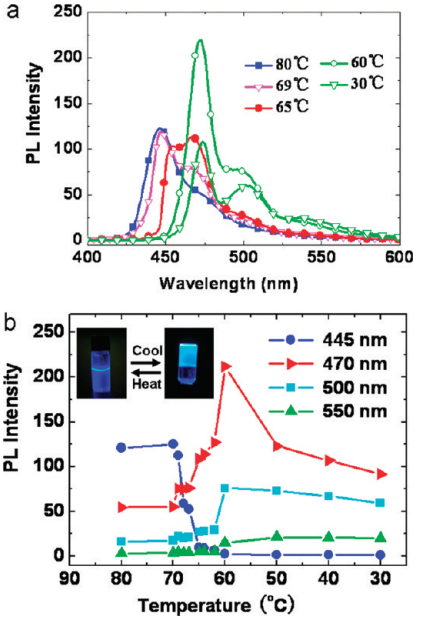

Figure 5. (a) Temperature-dependent PL spectra of PFO/DCE gel (blue line 80 °C, pink line 69 °C, red line 65 °C, and green group 60 and 30 °C). (b) Plot of PL intensity at 445, 470, 500, and 550 nm versus temperature. The inset shows the photograph of sol−gel transformation.

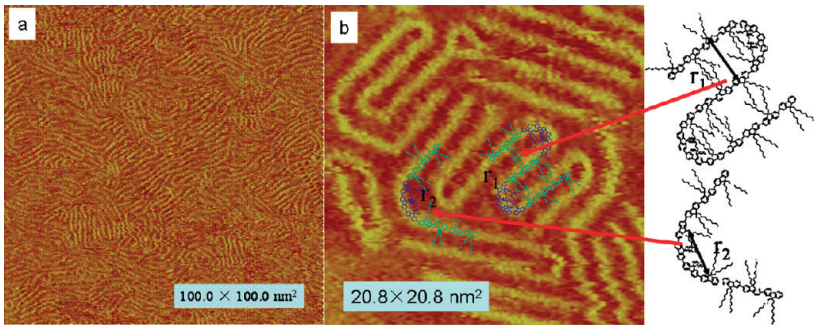

Figure 6. High-resolution STM image of the PFO on HOPG and the packing model of PFO, tunneling condition: −650 mV, 321 pA.

445 nm, which probably is attributed to the 0−0 transition of the β-phase, suggesting the existence of the β-phase with planar conformation. However, the nonexistence of the well-resolved sharp emission profile indicates the limited contents of β-phase in this state. The disappeared peak at 419 nm in dilute solution indicates that the content is enough to quench the high-energy emission of isotropic phase through the effective energy transfer. When the temperature was down to 69 °C, a new peak at 468 nm appeared obviously, besides the slight red shift of the 445 nm. Further decreasing the temperature to 65 °C, peak intensity of 468 nm is more than that of the first peak at 445 nm. When the temperature decreased to 60 °C, the complete different profile with three peaks of 473, 500, and 550 nm was observed. PL spectrum at the temperature of 60 °C has the same feature as that of PFO/DCE gel, which indicates the starting formation of gel network on the mesco-scale. The plot of PL intensities of a series of peaks at 445, 470, 500, and 550 nm versus temperature is summarized in Figure 5b. The range of transition took place from 69 to 60 °C, which is consistent with that of DSC at the range of 65−68 °C.

Formation Mechanism of PFO-SCPG. First, to understand further the self-assembly mechanism of PFO/DCE gelation system, we took advantage of STM to investigate the self-assembled monolayers (SAMs) of PFO at the solid−liquid interface.[64] The high-resolution STM images of the 2D layer of PFO at the highly oriented pyrolytic graphite (HOPG)−DCE interface are presented in Figure 6. It shows a large area lamellar structure with the well-defined self-assembled polymer strands. A high-resolution image indicates the conjugated backbone located at high bright region owing to higher tunneling probability associated with π-electrons.[65] The straight line image shows that the stiff rigid rod-type fluorene monomers take an alternate conformation similar to that of PFO β-phase. Bent shape with the higher bright contrast in some zones can be regarded as the folding chains owing to their relatively slower dynamics resulting from the restricted immobilization of conjugated backbones according to the literature reported by Mena-Osteritz et al.[64] The distance between polymer stands of 2.1 ± 0.1 nm (r_1) at a perfect hairpin folder was estimated to be four repeat units according to a 9,9-dioctylfluorene monomer with a length of 0.84 nm (inset of Figure 6b). Another folding length of ~2.7 ± 0.1 nm is equivalent to three or four repeat units of fluorene at the position of r_2. Furthermore, the width of grooves between the neighboring conjugated backbones is estimated to be ~1.1 nm, which is in good agreement with the interdigitations packing of octyl side chains between two adjacent blocks. The STM pictures of monolayers indicate that the isotropic phase of PFO with wormlike or rodlike conformations can be easily converted to a 2D single-layered β-sheet via the self-assembly of the side chains.[42,45,51]

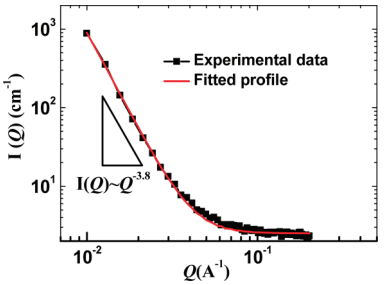

Figure 7. SAXS profiles of PFO/DCE gel obtained at room temperature and fitted curve with a model of cylinder.

Furthermore, PFO/DCE gel has been characterized by SAXS spectrum at room temperature. Figure 7 shows the SAXS profile in double-logarithmic plot. The lack of well-defined diffraction peaks indicates no long-range order in this physical network of PFO/DCE gel. The scattering intensity of the gel displays the power-law dependence of $Q^{-3.8}$ in the low-Q region ($q < 0.05$ Å^{-1}), which indicate rough surfaces. Furthermore, it suggests that this phase structure is dramatically different from sheet-like aggregates or the membrane phase of PFO/toluene gel with the power-law dependence of Q^{-2}.[45,51] A model of cylinder based on the nonlinear least-squares algorithm was adopted to fit the scattering profile of PFO/DCE gel, using eqs 1 and 2. As a result, the length (L) and the radius (R) of cylinder are 14.9 and 7.0 nm by the returned best fit, respectively. The corresponding radius of gyration (R_g) can be calculated as 6.6 ± 0.2 nm according to eq 3.[66] This result indicates that cylinder superstructures are key intermediates in the PFO/DCE gel.

A presumable formation model of the PFO/DCE gel is proposed in Figure 8. First, PFO with amorphous phase is difficult to dissolve in DCE with a concentration of 5 mg/mL at room temperature. After the heating at the temperature of 80 °C for several minutes, the PFO chains can dissolve in DCE solution into a mixture of the isotropic phase with the more extended wormlike conformation, linear rodlike chain, and the planar β-conformation with the low content.[41,67] During the cooling process, the β-phase content will greatly increase owing to the side-chain interactions.[68,69] When temperature decreases to 69−60 °C, the single-layered β-sheet can be smoothly converted from isotropic phase according to our STM results, followed by the formation of cylinder clusters with a thickness of 14.9 nm via the sheetlike aggregate by SAXS. Because cylinder clusters effectively dominated the PFO-enriched phase, the extensive cross-linked networks are formed by the phase separation with isotropic polymer chains. It should be noted that some

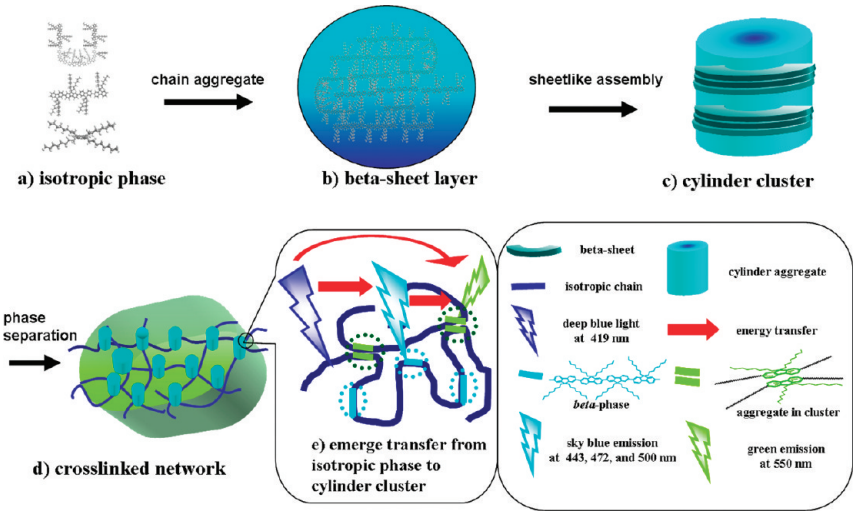

Figure 8. Schematic illustration of the formation mechanism of the PFO/DCE gel and its energy transfer processes.

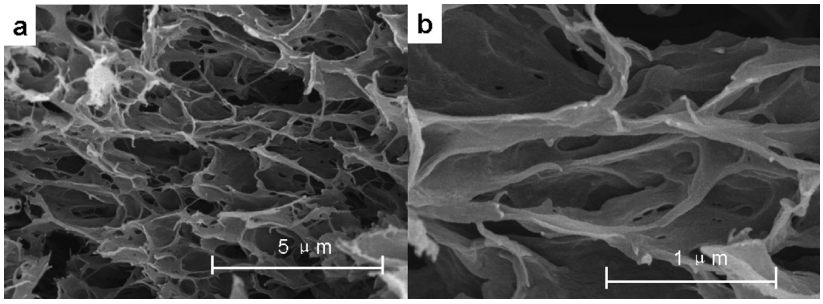

Figure 9. SEM images of a xerogel of PFO/DCE gel prepared by freeze-drying process.

chains in cylinder clusters exhibit very tight packing interaction of fluorene segments driven by the strong force to overcome the steric hindrance of dioctyl groups during the phase-separation process. In this framework, the unique PL of PFO/DCE gel can be explained (Figure 8e). The emission band at 470 nm in PFO/DCE gel originated from the effective energy transfer from the isotropic PFO chains to the cylinder clusters. Low-energy band at 550 nm is probably ascribed to the aggregate or excimer emission of π-stacked fluorene segments in cylinder clusters.

Microstructure of the Xerogel. Xerogel of PFO has been obtained by freeze-drying PFO/DCE gel at subambient temperature cooled by liquid nitrogen. SEM images of the xerogel showed a uniform sponge-like superstructure with regular pore size of 2−5 μm (Figure 9a). The wall of interpenetrated cavities is probably composed of PFO fiber networks with thickness of 100 nm according to Figure 9b. SAXS analysis of xerogel exhibits that there exist spherical-like scattered units with rough interfaces according to the Porod slope of ~3.8 and suggests a gyration radius of 21.6 nm from Guinier approximation. (See the Supporting Information.) These macroporous superstructures afford supporting evidence of the existence of mesomorphic phase of PFO/DCE gel with 3D networks. Well-ordered macroporous superstructures of PFO have been easily obtained by vacuum freeze-drying technology.[70] The frameworks of PFO/DCE gel can keep excellently during the macrophase separation when DCE as soft template is suddenly removed. This deduction can be confirmed by the PL spectra of xerogel, which is similar to that of PFO/DCE gel.

CONCLUSIONS

In summary, we have successfully prepared a supramolecular π-conjugated polymer gel of poly(9,9-dioctylfluorene) (PFO-SCPG) in DCE. PFO/DCE gel exhibits the content of β-phase up to 50% and the unique PL peaks at 470, 500, and 550 nm, which are dramatically distinguished from other polymorphisms. The green emissions at 550 nm in the PFO/DCE gel afford supporting evidence of the origination of low-energy green emission originated from the aggregate or excimer emission of π-stacked fluorene segments (called γ-phase) in PFs. The detained sol−gel transition process of PFO/DCE gel at ca. 60 °C has been monitored by temperature-resolved PL. The formation mechanism has been proposed based on the sequent intermediates, including single-layered β-sheet, cylinder cluster, and cross-linked network, which are supported by SAXS analysis of PFO/DCE gel and STM results of PFO at DCE−HOPG interface. Macroporous architectures of PFO obtained from the xerogel can be served as a promising candidate for the sensor and actuators.

EXPERIMENTAL SECTION

Chemicals and Materials. PFO end-capped with phenyl was synthesized by general Yamamoto coupling polycondensation.[71] PFO exhibits number-average molecular weight (M_n) of 6.94 × 10^4 with polydispersity (PDI) of 1.33 in this work by GPC analysis with PS standard. THF and diethyl ether were dried over

sodium benzophenone ketyl anion radical and distilled under a dry nitrogen atmosphere immediately prior to use.

Preparations of Solutions, Films, and Gel. The 5 mg·mL^{-1} DCE solution of PFO (Sol) was prepared by stirring the mixture at ca. 80 °C for 3 h, and a macroscopically homogeneous solution was observed by the naked eye. The PFO/DCE gel was prepared by aging the solutions at room temperature (~20 °C) for 24 h. PFO saturated solution was prepared by dissolving PFO (40 mg) into different solvents (2 mL) and refluxing for 3 h. Hot solution was filtrated through filter paper and then cooled to room temperature without stirring for 24 h. Aging PFO/DCE gel was obtained at room temperature in a sealed bottle for 1 month. The sample of xerogel was prepared by vacuum freeze-drying of the gel in liquid nitrogen for 12 h. The pristine film was spin-coated from 5 mg·mL^{-1} chloroform solution. Dip-processed film was prepared by dipping the pristine film in DCE for 20 s.

Characterization of PFO in Solution, Gel, Xerogel, And Film. The quartz cells of 10 mm thickness were used to measure the spectra of the dilute solutions, whereas for the semidilute viscous solution or gels, the samples were sandwiched between two quartz glasses to obtain the solution or gel layers of ~100 μm in thickness. Electronic absorption measurements were performed using Shimadzu UV-3600 spectrometer. The reported absorbance of the samples has been corrected for the solvent background. Fluorescence measurements were recorded for the same film with a Shimadzu RF-5301PC fluorometer with 390 nm excitation wavelength. The samples were placed in the quartz cell with a cubic rubber stopple. The temperature-dependent experiments were realized by using a thermostat tube heating system and measured as soon as possible when taken out from the water bathe. The concentrated solution was cool from 80 °C and kept 10 min at each temperature. IR spectra were recorded from 4000 to 800 cm^{-1} on an IR-Prestige-21 FT-IR spectrophotometer with a Mid-IR (MIR) globar source. The interferograms were recorded 32 times at the resolution of 4 cm^{-1}. A wideband mercury−cadmium−telluride (MCT) detector was used for the FT-IR measurement. DSC measurement was acquired using a Shimadzu Instruments DSC-60A. An aliquot of the PFO/DCE gel was used as the sample; a portion was placed in the pan. DSC data were collected from 30 to 80 °C at a rate of 5 °C/min for both the baseline and the sample, and the SEM images of xerogel were taken on a Hitachi S-4800 field-emission scanning electron microscope (FE-SEM) after a layer of gold was sputtered.

Small-Angle X-ray Scattering. The SAXS measurements were carried out on a NanoSTAR SAXS instrument from Bruker AXS. The instrument uses Cu Kα radiation (1.54 Å) produced in a sealed cathode tube with a typical current of 35 mA and a potential difference of 40 kV. The sample detector distance was set at 66.15 cm, covering a Q range of 0.01 to 0.20 Å^{-1}. The samples were placed in a sealed quartz capillary of ~1 mm path length. All measurements were carried out at ambient temperature without vacuum. Transmission was measured for 1800 s, and the scattering was measured for a sufficient amount of time to obtain at least 1 million counts on the detector.

SAXS from Cylinder Model.[72,73] The scattering intensity from a cylinder system, $I(Q)$, can be written as a function of the momentum transfer, Q, as

$$I(Q) = \int_0^{\pi/2} \left[\frac{\sin(1/2QL\cos\theta) \times 2J_1(QR\sin\theta)}{1/2QL\cos\theta \times QR\sin\theta}\right]^2 \sin\theta\, d\theta \quad (1)$$

where θ is the angle between the Q vector and cylinder axis, L is the length and R is the radius of the cylinder, and J_1 is the first-order Bessel function that can be written as

$$J_1(x) = \frac{1}{2\pi}\int_0^{2\pi} \exp[i(x\sin\theta - \theta)]\, d\theta \quad (2)$$

The parameters of gyration (R_g) describing the effective radius characteristics are related to the length (L) and the radius (R) of cylinder by

$$R_g^2 = \frac{L_2}{12} + \frac{R^2}{2} \quad (3)$$

Characterization of STM. The SAMs of the compounds were prepared by placing a drop (ca. 3 mL) of solution containing PFO (the concentration is ca. 10^{-4} mg/mL) on a freshly cleaved atomically flat surface of highly ordered pyrolytic graphite (HOPG, ZYB quality, Veeco Metrology). The samples were investigated at the liquid−solid interface. A Nanoscope *IIIa* scanning probe microscope (Veeco Metrology) was employed to carry out the STM experiments using a standard constant-current mode under ambient conditions. STM tips were mechanically cut Pt/Ir wire (80/20). All STM images shown herein are presented without further processing, except flattening. Experiments were repeated in several sessions using different tips to check for reproducibility and to avoid artifacts. The tunneling conditions used are given in the corresponding Figure captions.

■ ASSOCIATED CONTENT

Supporting Information. Fabrication and β-phase content calculation of DCE dip-processed film as well as a series of solvents; results discussed in the Results and Discussion that were omitted in the manuscript for the sake of brevity. This material is available free of charge via the Internet at http://pubs.acs.org.

■ AUTHOR INFORMATION

Corresponding Author

*E-mail: iamlhxie@njupt.edu.cn (L.-H.X.); wei-huang@njupt.edu.cn (W.H.).

■ ACKNOWLEDGMENT

The project was supported by the National Key Basic Research Program of China (973) (2009CB930600), National Natural Science Foundation of China (20774043, 20704023, 20974046, 60876010), Key Project of the Ministry of Education of China (707032, 208050), and Natural Science Foundation of Jiangsu Province (BK2008053, 10KJB510013, SJ209003).

■ REFERENCES

(1) Yan, H.; Chen, Z. H.; Zheng, Y.; Newman, C.; Quinn, J. R.; Dotz, F.; Kastler, M.; Facchetti, A. *Nature* **2009**, *457*, 679.

(2) Helgesen, M.; Sondergaard, R.; Krebs, F. C. *J. Mater. Chem.* **2009**, *20*, 36.

(3) Huang, W.; Meng, H.; Yu, W. L.; Gao, J.; Heeger, A. J. *Adv. Mater.* **1998**, *10*, 593.

(4) Yu, W. L.; Meng, H.; Pei, J.; Huang, W. *J. Am. Chem. Soc.* **1998**, *120*, 11808.

(5) Xie, L.-H.; Ling, Q.-D.; Hou, X.-Y.; Huang, W. *J. Am. Chem. Soc.* **2008**, *130*, 2120.
(6) Schenning, A. P. H. J.; Jonkheijm, P.; Hoeben, F. J. M.; van Herrikhuyzen, J.; Meskers, S. C. J.; Meijer, E. W.; Herz, L. M.; Daniel, C.; Silva, C.; Phillips, R. T.; Friend, R. H.; Beljonne, D.; Miura, A.; De Feyter, S.; Zdanowska, M.; Uji-i, H.; De Schryver, F. C.; Chen, Z.; Wurthner, F.; Mas-Torrent, M.; den Boer, D.; Durkut, M.; Hadley, P. *Synth. Met.* **2004**, *147*, 43.
(7) Chen, L. M.; Hong, Z. R.; Li, G.; Yang, Y. *Adv. Mater.* **2009**, *21*, 1434.
(8) Allard, S.; Forster, M.; Souharce, B.; Thiem, H.; Scherf, U. *Angew. Chem., Int. Ed.* **2008**, *47*, 4070.
(9) Redecker, M.; Bradley, D. D. C.; Inbasekaran, M.; Woo, E. P. *Appl. Phys. Lett.* **1999**, *74*, 1400.
(10) Chunwaschirasiri, W.; Tanto, B.; Huber, D. L.; Winokur, M. J. *Phys. Rev. Lett.* **2005**, *94*, 107402.
(11) Chen, S. H.; Chou, H. L.; Su, A. C.; Chen, S. A. *Macromolecules* **2004**, *37*, 6833.
(12) Chen, S. H.; Su, A. C.; Su, C. H.; Chen, S. A. *Macromolecules* **2005**, *38*, 379.
(13) Abbel, R.; Schenning, A.; Meijer, E. W. *J. Polym. Sci., Polym. Chem.* **2009**, *47*, 4215.
(14) O'Carroll, D.; Iacopino, D.; O'Riordan, A.; Lovera, P.; O'Connor, E.; O'Brien, G. A.; Redmond, G. *Adv. Mater.* **2008**, *20*, 42.
(15) Wu, C. F.; McNeill, J. *Langmuir* **2008**, *24*, 5855.
(16) O'Carroll, D.; Lieberwirth, I.; Redmond, G. *Nat. Nanotechnol.* **2007**, *2*, 180.
(17) Suzuki, M.; Hanabusa, K. *Chem. Soc. Rev.* **2010**, *39*, 455.
(18) Shi, N. E.; Dong, H.; Yin, G.; Xu, Z.; Li, S. H. *Adv. Funct. Mater.* **2007**, *17*, 1837.
(19) Sangeetha, N. M.; Maitra, U. *Chem. Soc. Rev.* **2005**, *34*, 821.
(20) George, M.; Weiss, R. G. *Acc. Chem. Res.* **2006**, *39*, 489.
(21) Estroff, L. A.; Hamilton, A. D. *Chem. Rev.* **2004**, *104*, 1201.
(22) Yang, Z.; Liang, G.; Xu, B. *Acc. Chem. Res.* **2008**, *41*, 315.
(23) John, G.; Zhu, G. Y.; Li, J.; Dordick, J. S. *Angew. Chem., Int. Ed.* **2006**, *45*, 4772.
(24) Li, J. L.; Wang, R. Y.; Liu, X. Y.; Pan, H. H. *J. Phys. Chem. B* **2009**, *113*, 5011.
(25) Lehn, J. M. *Chem. Soc. Rev.* **2007**, *36*, 151.
(26) Daniel, C.; Avallone, A.; Guerra, G. *Macromolecules* **2006**, *39*, 7578.
(27) Saiani, A.; Guenet, J.-M. *Macromolecules* **1997**, *30*, 966.
(28) Pich, A.; Schiemenz, N.; Boyko, V.; Adler, H. J. P. *Polymer* **2006**, *47*, 553.
(29) Vijayakumar, C.; Praveen, V. K.; Ajayaghosh, A. *Adv. Mater.* **2009**, *21*, 2059.
(30) Wicklein, A.; Ghosh, S.; Sommer, M.; Wurthner, F.; Thelakkat, M. *ACS Nano* **2009**, *3*, 1107.
(31) Matsumoto, A.; Sato, N.; Sakata, T.; Yoshida, R.; Kataoka, K.; Miyahara, Y. *Adv. Mater.* **2009**, *21*, 4372.
(32) Hong, J. P.; Um, M. C.; Nam, S. R.; Hong, J. I.; Lee, S. *Chem. Commun.* **2009**, 310.
(33) Landau, O.; Rothschild, A.; Zussman, E. *Chem. Mater.* **2009**, *21*, 9.
(34) Osada, Y.; Okuzaki, H.; Hori, H. *Nature* **1992**, *355*, 242.
(35) Trigueiro, J. P. C.; Borges, R. S.; Lavall, R. L.; Calado, H. D. R.; Silva, G. G. *Nano Res.* **2009**, *2*, 733.
(36) Kang, B.; Ceder, G. *Nature* **2009**, *458*, 190.
(37) Morita, S.; Shakuda, S.; Sugimoto, R.; Yoshino, K. *Synth. Met.* **1993**, *55*, 1182.
(38) Malik, S.; Jana, T.; Nandi, A. K. *Macromolecules* **2000**, *34*, 275.
(39) Chen, S. H.; Su, A. C.; Chang, C. S.; Chen, H. L.; Ho, D. L.; Tsao, C. S.; Peng, K. Y.; Chen, S. A. *Langmuir* **2004**, *20*, 8909.
(40) Ajayaghosh, A.; Praveen, V. K. *Acc. Chem. Res.* **2007**, *40*, 644.
(41) Grell, M.; Bradley, D. D. C.; Long, X.; Chamberlain, T.; Inbasekaran, M.; Woo, E. P.; Soliman, M. *Acta Polym.* **1998**, *49*, 439.
(42) Chen, J. H.; Chang, C. S.; Chang, Y. X.; Chen, C. Y.; Chen, H. L.; Chen, S. A. *Macromolecules* **2009**, *42*, 1306.
(43) Knaapila, M.; Almasy, L.; Garamus, V. M.; Ramos, M. L.; Justino, L. L. G.; Galbrecht, F.; Preis, E.; Scherf, U.; Burrows, H. D.; Monkman, A. P. *Polymer* **2008**, *49*, 2033.
(44) Barton, A. F. M. *Chem. Rev.* **1975**, *75*, 731–753.
(45) Knaapila, M.; Garamus, V. M.; Dias, F. B.; Almasy, L.; Galbrecht, F.; Charas, A.; Morgado, J.; Burrows, H. D.; Scherf, U.; Monkman, A. P. *Macromolecules* **2006**, *39*, 6505.
(46) Kitts, C. C.; Vanden Bout, D. A. *Polymer* **2007**, *48*, 2322 .
(47) Khan, A. L. T.; Sreearunothai, P.; Herz, L. M.; Banach, M. J.; Kohler, A. *Phys. Rev. B* **2004**, *69*, 8.
(48) Chen, S. H.; Su, A. C.; Chen, S. A. *J. Phys. Chem. B* **2005**, *109*, 10067.
(49) Zhu, R.; Lin, J. M.; Wang, W. Z.; Zheng, C.; Wei, W.; Huang, W.; Xu, Y. H.; Peng, J. B.; Cao, Y. *J. Phys. Chem. B* **2008**, *112*, 1611.
(50) Peet, J.; Brocker, E.; Xu, Y. H.; Bazan, G. C. *Adv. Mater.* **2008**, *20*, 1882.
(51) Knaapila, M.; Stepanyan, R.; Torkkeli, M.; Garamus, V. M.; Galbrecht, F.; Nehls, B. S.; Preis, E.; Scherf, U.; Monkman, A. P. *Phys. Rev. E* **2008**, *77*, 14.
(52) Dias, F. B.; Morgado, J.; Macanita, A. L.; da Costa, F. P.; Burrows, H. D.; Monkman, A. P. *Macromolecules* **2006**, *39*, 5854.
(53) Lu, H. H.; Liu, C. Y.; Jen, T. H.; Liao, J. L.; Tseng, H. E.; Huang, C. W.; Hung, M. C.; Chen, S. A. *Macromolecules* **2005**, *38*, 10829.
(54) Liu, L. L.; Lu, P.; Xie, Z. Q.; Wang, H. P.; Tang, S.; Wang, Z. M.; Zhang, W.; Ma, Y. G. *J. Phys. Chem. B* **2007**, *111*, 10639.
(55) Yang, X. H.; Jaiser, F.; Neher, D.; Lawson, P. V.; Bredas, J. L.; Zojer, E.; Guntner, R.; de Freitas, P. S.; Forster, M.; Scherf, U. *Adv. Funct. Mater.* **2004**, *14*, 1097.
(56) Chen, X. W.; Tseng, H. E.; Liao, J. L.; Chen, S. A. *J. Phys. Chem. B* **2005**, *109*, 17496.
(57) Koizumi, Y.; Seki, S.; Tsukuda, S.; Sakamoto, S.; Tagawa, S. *J. Am. Chem. Soc.* **2006**, *128*, 9036.
(58) Jaramillo-Isaza, F.; Turner, M. L. *J. Mater. Chem.* **2006**, *16*, 83.
(59) Panozzo, S.; Vial, J. C.; Kervella, Y.; Stephan, O. *J. Appl. Phys.* **2002**, *92*, 3495.
(60) Liu, L. L.; Tang, S.; Liu, M. R.; Xie, Z. Q.; Zhang, W.; Lu, P.; Hanif, M.; Ma, Y. G. *J. Phys. Chem. B* **2006**, *110*, 13734.
(61) Gong, X. O.; Iyer, P. K.; Moses, D.; Bazan, G. C.; Heeger, A. J.; Xiao, S. S. *Adv. Funct. Mater.* **2003**, *13*, 325.
(62) Wang, P. S.; Lu, H. H.; Liu, C. Y.; Chen, S. A. *Macromolecules* **2008**, *41*, 6500.
(63) Herz, L. M.; Phillips, R. T. *Phys. Rev. B* **2000**, *61*, 13691.
(64) Mena-Osteritz, E. *Adv. Mater.* **2002**, *14*, 609.
(65) Samori, P.; Severin, N.; Mullen, K.; Rabe, J. P. *Adv. Mater.* **2000**, *12*, 579.
(66) Roe, R. *Methods of X-Ray and Neutron Scattering in Polymer Science*; Oxford University Press: Oxford, U.K., 2000.
(67) Fytas, G.; Nothofer, H. G.; Scherf, U.; Vlassopoulos, D.; Meier, G. *Macromolecules* **2002**, *35*, 481.
(68) Knaapila, M.; Dias, F. B.; Garamus, V. M.; Almasy, L.; Torkkeli, M.; Leppanen, K.; Galbrecht, F.; Preis, E.; Burrows, H. D.; Scherf, U.; Monkman, A. P. *Macromolecules* **2007**, *40*, 9398.
(69) Rahman, M. H.; Chen, C. Y.; Liao, S. C.; Chen, H. L.; Tsao, C. S.; Chen, J. H.; Liao, J. L.; Ivanov, V. A.; Chen, S. A. *Macromolecules* **2007**, *40*, 6572.
(70) Zuo, Z. C.; Guo, Y. B.; Li, Y. L.; Lv, J.; Liu, H. B. A.; Xu, J. L.; Li, Y. J. *Macromol. Rapid Commun.* **2009**, *30*, 1940.
(71) Grell, M.; Knoll, W.; Lupo, D.; Meisel, A.; Miteva, T.; Neher, D.; Nothofer, H. G.; Scherf, U.; Yasuda, A. *Adv. Mater.* **1999**, *11*, 671.
(72) Pedersen, J. S.; Schurtenberger, P. *Macromolecules* **1996**, *29*, 7602.
(73) Glatter, O. *J. Appl. Crystallogr.* **1977**, *10*, 415.